ACS OMEGA

Article

http://pubs.acs.org/journal/acsodf

Biocomposites with Size-Fractionated Biocarbon: Influence of the Microstructure on Macroscopic Properties

Vidhya Nagarajan,[†,‡] Amar K. Mohanty,*[,†,‡] and Manjusri Misra[†,‡]

[†]College of Physical and Engineering Sciences, School of Engineering, Thornborough Building and [‡]Bioproducts Discovery and Development Centre, Department of Plant Agriculture, Crop Science Building, University of Guelph, 50 Stone Road East, Guelph, N1G 2W1 Ontario, Canada

Supporting Information

ABSTRACT: This study is an experimental investigation of using biocarbon as renewable carbonaceous filler for engineering-plastic-based blends. Poly(trimethylene terephthalate) (PTT) and poly(lactic acid) (PLA) combined with a terpolymer were selected as the blend matrix. Biocarbon with various particle size ranges was segregated and used as filler. Depending on the particle size and aspect ratio of the biocarbon used, the microstructure of the composite was found to change. Composites having a biocarbon particle size range of 20−75 μm resulted in a morphology showing better dispersion of the blend components when compared with composites containing other biocarbon particle size ranges. Furthermore, the addition of epoxy-based multifunctional chain extender was found to result in much finer morphologies having dispersed polymer particles of very small size. Impact strength increased significantly in composites that possessed such morphologies favoring high energy dissipation mechanisms. A maximum notched Izod impact strength of 85 J/m was achieved in certain composite formulations, which is impressive considering the inherent brittleness of PTT and PLA. From rheological observations, incorporation of biocarbon increased viscosity, but the shear-thinning behavior of the matrix was preserved. By increasing the injection mold temperature, fast crystallization of PTT was achieved, which increased the heat deflection temperature of composites to 80 °C. This study shows that composites with overall improvement in mechanical and thermal performance can be produced by selecting biocarbon with appropriate particle sizes and suitable processing aids and conditions, which all together control the morphology and crystallinity.

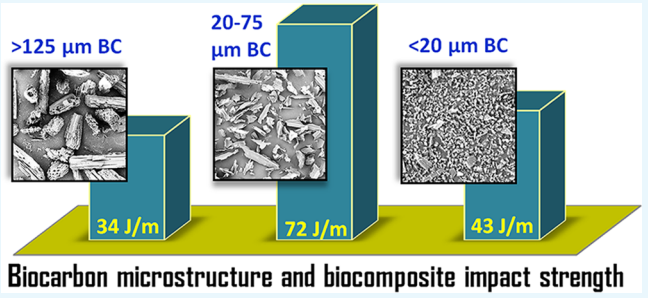

INTRODUCTION

Warming of the planet is unequivocal. Leading scientific organizations worldwide endorse that climate change is real; related resources can be found on NASA's Web page on global climate change.[1] Intensive research and development efforts are therefore focused on using carbon strategically, without emitting more greenhouse gases and causing extensive environmental damage. Biochar is a solid material obtained from thermochemical conversion of biomass in an oxygen-limited environment.[2] Research findings on biochar (i.e., biocarbon) and their practical implementation are increasing exponentially. The carbon contained in the biomass, taken from the atmosphere in the form of CO_2 during plant growth, is stored for a long period of time in biochar, making it an excellent source for carbon sequestration. Although biochar was initially designated for use in soil amendments, it is being applied in a cascade of areas now including water treatment, animal farming, construction, and composite materials.[3] The term *biocarbon* has been introduced to emphasize its application as filler or a reinforcing agent in composites, distinguishing it from carbon black.

Biocarbon has a relatively high surface area and carbon content (50%−80%) and is hydrophobic when compared with natural fibers, which makes it a desirable filler for composites.[4] Biocarbon can also act as a reinforcement based on its aspect ratio, strength, and stiffness. It offers a wide processing window for blending with engineering plastics, unlike most other natural fibers that degrade above 200 °C. The thermal stability of the resulting composites is higher when compared with that of the composites with natural fibers, for example, polypropylene (PP)/jute fiber, PP/wood fiber, and PLA/flax fiber composites. Issues related to the unpleasant odor associated with lignocellulosic natural fibers are greatly minimized while using biocarbon because it contains very little lignocellulosic components that usually give rise to the undesirable odor. Similar to carbon black, a widely used petroleum-based colorant, biocarbon can also act as a colorant in materials targeted for automotive and electronic applications. With all of these favorable and functional attributes, biocarbon-based composites can provide significant opportunities for weight saving, strength, and versatility in automotive interior parts. This will allow automakers to meet stringent fuel standards

Received: August 8, 2016
Accepted: October 5, 2016
Published: October 20, 2016

DOI: 10.1021/acsomega.6b00175
ACS Omega 2016, 1, 636−647

without sacrificing the performance, quality, and safety. However, only limited research has been conducted in promoting biocarbon-based composites for such applications. Peterson et al.[5−7] and Jong et al.[8] investigated biocarbon from different sources with varying carbon content and particle size as a potential replacement for carbon black in styrene butadiene rubber and natural rubber. Characterization of biocarbon from different sources[9] and surface treatment[10] have been carried out to promote the use of biocarbon for composite applications. Polytrimethylene terephthalate (PTT),[11,12] nylon,[13,14] epoxy,[15] polyvinyl alcohol (PVA),[16] and PP[17] are some of the matrices in which the effect of biocarbon has been investigated. Recently, Das et al.[18−20] have published a series of research articles on using biocarbon in combination with wood flour to develop "wood plastic biochar composites". Although the original driving force for adding fillers to polymers was to reduce the overall cost of the final formulations, fillers also modify certain properties of the matrix favorably. All of the above published literature agrees with the stiffening effect of biocarbon. Key understanding underpinning the information is that these publications show the importance of carbon content, particle size, pyrolysis temperature, and surface area in enhancing the performance of the biocarbon composites.

The aim of the current study was to investigate the effect of size-fractionated biocarbon on the resulting morphology and macroscopic properties of the composites, which would enable the selection of biocarbon with appropriate sizes and aspect ratio for target applications. A PTT−PLA blend moderately toughened with ethylene methyl acrylate glycidyl methacrylate (EMAGMA) was selected as the matrix material. PTT is a semi-crystalline polymer produced from the condensation of propylene diol (PDO) with terephthalic acid or dimethyl terephthalate, joining the PET (polyethylene terephthalate) and PBT (polybutylene terephthalate) family of polyesters. PLA remains one of the most widely researched biopolymers and is increasingly seen blended with other durable engineering polymers to widen their application areas. However, both PTT and PLA have poor impact resistance; hence, they are blended with EMAGMA to improve their impact strength. On the basis of the statistical optimization of the blending process performed in our previous study,[21] PTT−PLA/EMAGMA (85/15) blend was selected as the matrix. The ratio of PTT/PLA was kept constant at 70:30 wt %. Our previous investigation[21] also showed that only the impact strength was significantly affected in the presence of chain extender, owing to the changes in blend morphology. As one of the aims of the current study was to investigate the effect of chain extender on the composite system, blends without chain extender were considered for baseline comparison. By adding biocarbon to the PTT−PLA/EMAGMA matrix, cost-effective composite formulations can be developed if favorable properties are obtained. The cost of biocarbon is expected to be significantly cheaper than that of the matrix system but varies based on the raw material used for its production. For example, if the biocarbon is produced from baled miscanthus, as in this study, the cost would depend on the cost of miscanthus and the biocarbon production cost. If the biocarbon is produced from a coproduct, which currently does not have any market value, then the cost will include only the cost associated with the production process (thermal conversion) and hence will be significantly much cheaper. As both PTT and PLA have low impact strength and heat resistance, the goal of this study was to develop a formulation that will show improvement in the above-mentioned properties, relative to the neat polymers and with cost advantages. Because of the general tendency of fillers to reduce the impact strength at a higher filler content, the preliminary investigation reported here was conducted by adding only 10 wt % biocarbon. The effect of different size-fractionated biocarbon particles obtained through mechanical sieving was investigated by studying the microstructure, mechanical, thermal, and rheological properties. The effect of adding a chain extender and increasing the mold temperature was also investigated. Final properties of the composites are critically dependent on the size, shape, and aspect ratio of the particles themselves. Therefore, particle size distributions through image analysis for different size-fractionated biocarbon particles were also analyzed.

EXPERIMENTAL SECTION

Materials. PTT available under the trade name Sorona 3301 BK 001 was kindly supplied by DuPont (Wilmington, DE, USA). This grade of Sorona used contains 35 wt % of the renewable resource content derived from corn. NatureWorks Ingeo PLA 3001D with 1.5% D-lactide content was supplied by NatureWorks LLC (Minnetonka, MN, USA). Lotader AX 8900 (EMAGMA) product of Arkema (Colombes, France) was purchased from Quadra Chemicals, Canada. Epoxy-functionalized chain extender (CE) used in this study was Joncryl ADR-4368, a product of BASF (Ludwigshafen, Germany). Miscanthus-based biocarbon (BC) hammer milled to ∼400 μm (1/64 in.) was received from Competitive Green Technologies, Leamington, ON, Canada. This biocarbon was produced through a low-temperature pyrolysis process, as the functionalities are noticed to be still present in the FTIR spectra, as shown in the Supporting Information. Before processing, a 12 h drying protocol for PTT at 105 °C, for PLA at 80 °C, and for EMAGMA at 60 °C was followed. The moisture content of the polymers before processing was measured to be 0.045 ± 0.007%. The moisture content of the biocarbon stored in the oven at 105 °C was measured to be 1.6 ± 0.15%.

Size-Fractionation of Biocarbon. Size-fractionation of biocarbon was performed using a nest of WS Tyler test sieves having openings of 300, 212, 150, 125, 75, and 20 μm. The coarse and fine sieves were assembled on a Ro-tap sieve shaker (WS Tyler, OH, USA) and agitated for 10 min. Schematic of the sieve setup is shown in Figure 1 along with the particle size range selected for this study.

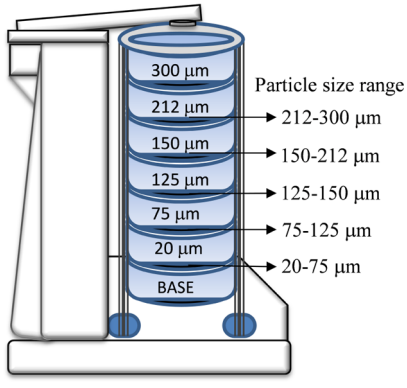

Figure 1. Schematic of the sieve setup on a Ro-Tap sieve shaker.

DOI: 10.1021/acsomega.6b00175
ACS Omega 2016, 1, 636−647

After the sieving was complete, the mass retained over different sieves was collected, weighed, and analyzed. Percentage of mass retained on each sieve was calculated from three replications of sieving. To obtain a substantial amount of biocarbon below 20 μm, "as-received", biocarbon was further subjected to ball milling for 3 h at 300 rpm. Planetary ball mill (Retsch GmbH, Haan, Germany) was used for size reduction. The stainless steel grinding jar was charged with 40 g of biocarbon, and the milling media contained 64 small zirconium oxide balls of diameter 10 mm and 1 stainless steel ball of diameter 40 mm. The milled biocarbon was then sieved using the Retsch air jet sieving machine AS 200 to obtain biocarbon primarily below 20 μm. Sieving time and speed were set to 1 min and 30 rpm, respectively.

Biocomposite Fabrication. Biocomposites were fabricated in a microcompounder (DSM Xplore, the Netherlands) by adding all of the blend components and size-fractionated biocarbon of required composition in a one-step process. The length and the L/D ratio of the screws were 150 and 18 mm, respectively. The barrel volume of the machine was 15 cm^3. Extrusion was performed at 250 °C barrel temperature and 200 rpm screw speed. After a total residence time of 2 min, a preheated collector with a piston cylinder assembly was used to transfer the molten extrudate into a DSM micro 12 cc injection molding machine, without pelletization. The injection pressure for injection and holding stages was set at 4 and 8 bar, respectively; the total injection time was 18 s. Samples were molded at 30 °C mold temperature. For selected biocomposites, samples were also molded at 60 and 90 °C. The injection time was increased to 60 s to facilitate cooling and easy sample removal without distortion when a high mold temperature was used. The effect of chain extender and mold temperature was investigated only in composites with 20−75 μm BC and less than 20 μm BC for concise presentation of the experimental results. Mold temperatures of 30, 60, and 90 °C were adopted for 20−75 μm BC composites. On the basis of the initial assessment of the mechanical properties and heat resistance of these composites, only 30 and 90 °C were selected to investigate BC composites less than 20 μm. To show the effect of chain extender (CE) in combination with the mold temperature, the CE was added to 20−75 μm BC composites molded at 30 and 90 °C. For comparison, the properties of less than 20 μm BC composites containing CE molded only at 90 °C are provided.

Testing and Characterization. *Morphology and Particle Size Measurement.* The morphology of individual biocarbon particles and fractured surface was observed using the scanning electron microscope Phenom ProX (Phenom World BV, the Netherlands) equipped with a back scattering electron (BSE). Cressington sputter coater 108 was used to gold-coat the composite samples for 15 s under an argon atmosphere. Selected composites were etched in chloroform for 30 min at 50°C to remove the PLA and EMAGMA phase. ImageJ, a public domain image processing and analysis program developed by the National Institutes of Health (NIH), USA, was used to measure the particle size of biocarbon. Around 300 particles were measured in the longest and the shortest dimensions for biocarbon above 75 μm. For 20−75 μm BC and less than 20 μm BC, around 1000 particles were measured for the longest dimension.

Mechanical Properties and Rheology. Mechanical properties were measured after the test specimens were conditioned in the standard laboratory atmosphere for 48 h at 23 °C and 50% relative humidity (ASTMD618-08, procedure A). Instron Instrument Model 3382 was used to study the tensile and flexural properties of the biocomposites. ASTM standard D638 with type IV sample was followed for the tensile test. The flexural test was performed following the ASTM D790 procedure B. The tensile properties of biocomposites were tested at 5 mm/min. The flexural specimens were tested at a crosshead speed of 14 mm/min. Notched Izod impact strength was measured with the help of Testing Machine Inc. (TMI) instrument, according to ASTM D256. At least six notched samples were measured for impact strength and five samples for tensile and flexural properties. Average values with standard deviations are reported.

Rheological characterization was conducted using an Anton Paar MCR302 rheometer (Anton Paar GmbH, Graz, Austria) using a parallel plate configuration. The plate diameter used was 25 mm, with a measurement gap distance set at 1 mm. The shear rate was varied between 0.01 and 1000/s. The test was conducted at 250 °C under a nitrogen purge.

Differential Scanning Calorimetry (DSC). DSC was performed by heating the samples to 240 °C with a heating rate of 10 °C/min, followed by a 3 min isothermal step to erase the thermal history, and then cooled to −50 °C with a cooling rate of 5 °C/min. The same heating profile was used for the second heating scan as well. Glass transition temperature (T_g), cold crystallization temperature (T_{cc}), crystallization temperature (T_c), and melting temperature (T_m) were determined from the DSC graphs. Percentage crystallinity (χ_c) was calculated using the equation

$$\chi_c = \frac{\Delta H_m - \Delta H_{cc}}{f \Delta H_m^0} \times 100\%$$

where ΔH_m is the enthalpy of melting, ΔH_{cc} is enthalpy of cold crystallization, and ΔH_m^0 is the enthalpy of melting of 100% pure PTT, 145.5 J/g.[22] f is the weight fraction of PLA in the blend. Results reported are the average values of at least two samples.

Dynamic Mechanical Analysis (DMA). DMA was conducted on DMA Q800 from TA Instruments using a dual-cantilever clamp in a frequency sweep/temperature ramp mode at the frequency of 1 Hz and oscillating amplitude of 15 μm. The samples (dimensions 12.7 × 63.5 × 3.2 mm^3) were heated from −50 to 120 °C at a heating rate of 3 °C/min. Heat deflection temperature (HDT) was also measured using DMA Q 800 with a three-point bending clamp in the DMA controlled force mode at a stress of 0.455 MPa and a ramp rate of 2 °C/min.[11,13] Deflection was evaluated at 0.1889% strain.

RESULTS AND DISCUSSION

Particle Size Analysis and Shape Classification. Particle size distribution (PSD) from the sieve shaker provides the percentage of particles retained on different-sized sieves as shown in Figure 2. A maximum weight percentage distribution was achieved in the range of 20−75 μm. Hammer mill is known to break down the biomass or in this case biocarbon because of the action of shear and friction. Milling screen size, motor speed, and material feeding method are mentioned to be key variables determining the resulting particle size and particle size distribution.[23] As seen from Figure 2, this kind of distribution provides a broad range of particle size based on the selected sieve. Therefore, particle sizes in the longest and the shortest

DOI: 10.1021/acsomega.6b00175
ACS Omega 2016, 1, 636−647

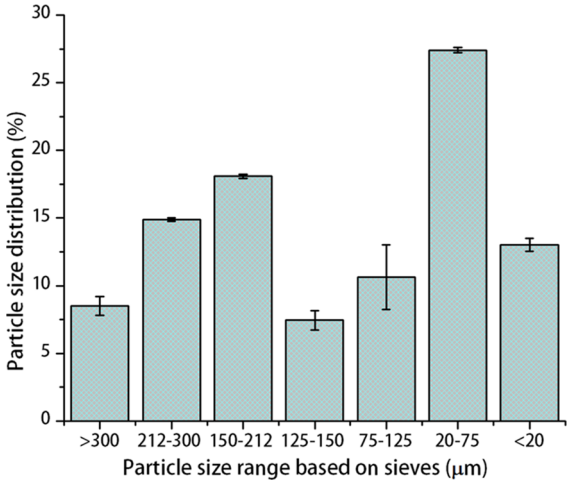

Figure 2. Particle size distribution based on the mass retained in the sieves.

dimensions within each of these ranges were measured from SEM images.

In addition to providing relatively precise particle size distribution, SEM can also provide useful information regarding the shape of the particles. Representative SEM images used for the analysis are shown in Figure 3. Particle size distribution is presented in Figures 4 and 5. Size-fractionated biocarbons are differentiated based on the sieve openings.

The shape of the biocarbon in the first four particle size ranges above 75 μm resembles the structure of chopped miscanthus fibers from which the biocarbon was pyrolyzed. On the basis of the ASTM standard F1877-05 (appendix ×2),[24] they could be classified under "sharps or shards—rectangular fibers". Particles of biocarbon in the 20−75 μm range have sharp edges and can be called "sharps or shards—cuttlefish". The shape of the particles less than 20 μm can be described to be a mixture of "granular, irregular—smooth and angulated". Broad particle size distribution can be observed for particle length (the longest dimension) when compared with particle width (the shortest dimension) distribution histograms shown in Figure 4. This can be explained based on the characteristics of mechanical sieving. In general, the sieving process is described as a width-based separation process, where the particles having width higher than the sieve-opening size cannot pass through in any given orientation.[25] However, when the sieves are under tapping motion, longer particles can "fall-through" or "nose-dive" into smaller sieve openings.[25] This tipping action results in larger inconsistencies in length-based separation processes, which is reflected as a broad distribution when the particle length is measured. Particles having dimensions much higher than the maximum sieve opening can be observed from Figure 4. However, as the sieve-opening size reduces, the distribution becomes narrower. Although majority of the particle width is within the sieve-opening range, the presence of smaller particles cannot be avoided as they tend to agglomerate and cling to one another during sieving. Only length-based particle size distribution is provided for 20−75 μm and less than 20 μm sieve in Figure 5 because of the difficulty in measuring the width for the particles laying edge-wise showing thickness, the third dimension. Also, as the particle size reduces, the length of the granular-shaped particles coincides with their width. Majority of the BC belonging to the 20−75 μm sieve range has a particle length of less than 75 μm.

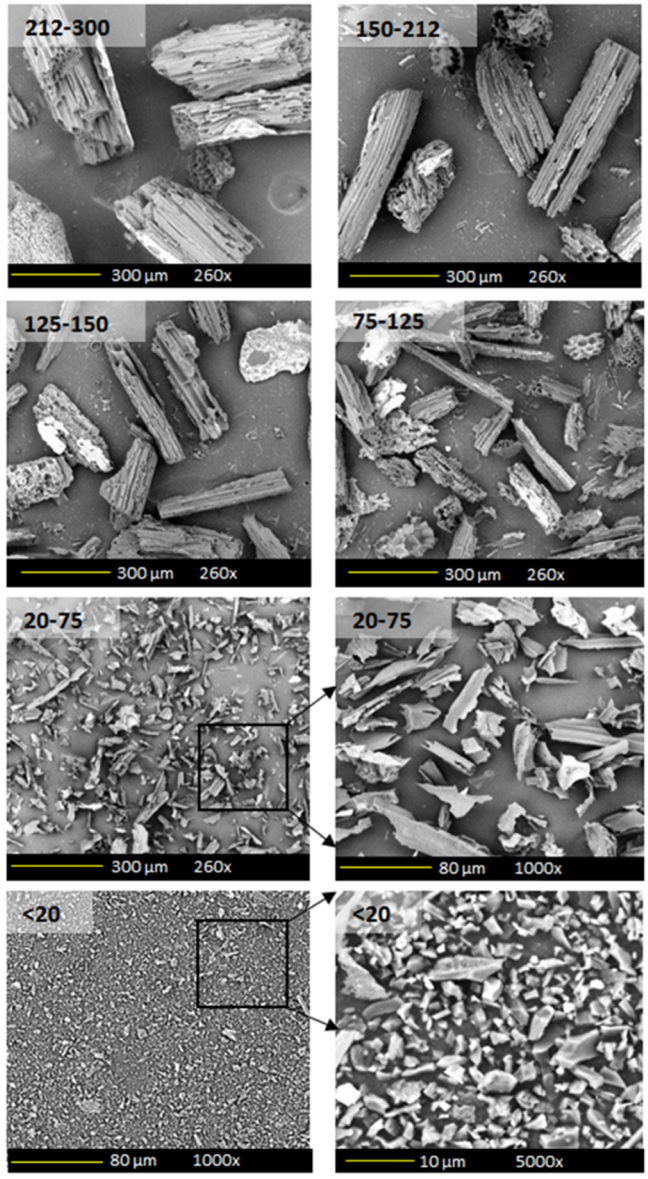

Figure 3. SEM images of biocarbon sieved to different particle size ranges.

The size-fractionation process through mechanical sieving resulted in lesser amounts of biocarbon below 20 μm (Figure 2); therefore, to obtain a substantial amount of biocarbon in this range to fabricate composites, "as-received" biocarbon was subjected to the ball-milling process (conditions described in the Experimental Section). The milled biocarbon was sieved to below 20 μm without fractionation in an air jet sieve. Majority of the BC particles were smaller than 2 μm, indicating that the ball milling process has resulted in greater size reduction. This also explains the shape of these particles being quite different from other biocarbon particles of higher sieve-opening ranges. Such differences in shapes, sizes, and hence, the aspect ratio of the biocarbon are expected to have a significant effect on the matrix, resulting in different morphologies and macroscopic properties.

Morphology. Impact-fractured surface morphology of composites containing different size-fractionated biocarbon particles is shown in Figures 6 and 7. Biocarbon particles are randomly oriented in planes parallel to the surface and are

DOI: 10.1021/acsomega.6b00175
ACS Omega 2016, 1, 636−647

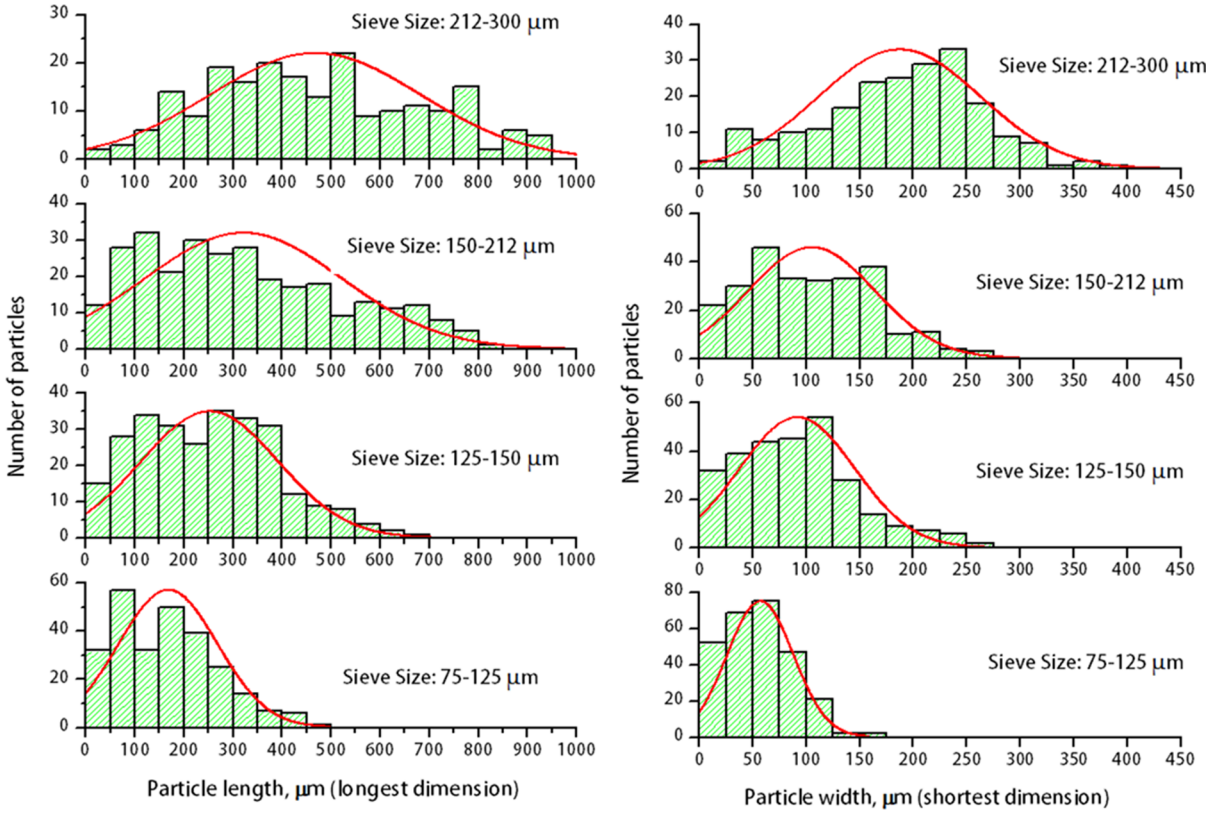

Figure 4. Particle size distribution along the longest and the shortest dimensions for size-fractionated BC.

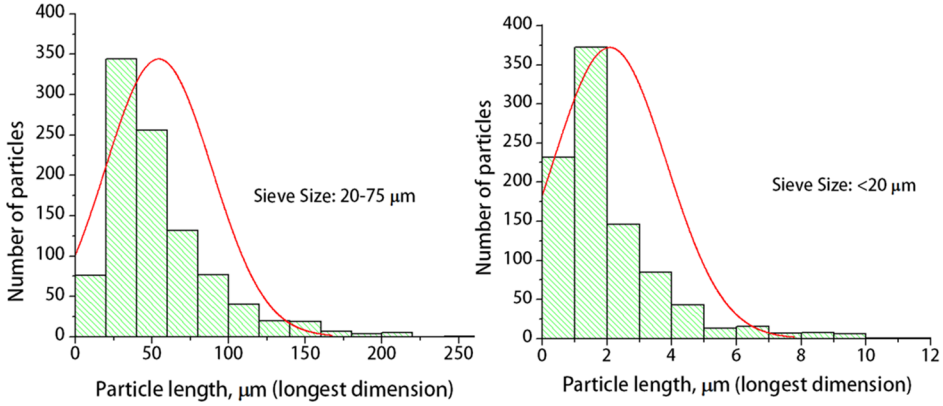

Figure 5. Particle size distribution along the longest dimension for 20−75 and <20 μm BC.

visibly well-distributed over the entire section of the matrix for composites shown in Figure 6. Morphology of the matrix in composites with biocarbon above 125 μm does not show any phase-separated blend components, PLA and EMAGMA. With reduction in BC particle size to less than 125 μm, roughly spherical domains of dispersed PLA−EMAGMA are noticed, where the blend retains its sea-island morphology. This morphology is predominant in composites with 75−125 and 20−75 μm ranges and can be viewed from the higher magnification section. For composites with less than 20 μm BC, the morphology changes again from a sea-island structure to a morphology with elongated bands of coalesced PLA−EMAGMA as shown in Figure 7. To clearly present the change in composite microstructure, the fractured surfaces were etched in chloroform at 50 °C for 30 min. Chloroform etched both PLA and EMAGMA phases, leaving the PTT phase intact. In Figure 7c,d, etched images of these composites are presented in a lower magnification when compared with images in Figure 7a,b to show the distinct difference.

The flow-induced microstructure changes continuously because of a complex interplay between breakup and coalescence. In composites with less than 20 μm biocarbon, the bands are made of coalesced PLA and EMAGMA particles. This difference in morphology could be attributed to the change in (i) viscosity, (ii) biocarbon particle shape with milling and associated changes in packing fractions, or (iii) free energy of mixing, which alters the interaction and interfacial tension between the blend components. These results demonstrate that the morphology of the composites is contingent not only on the particle size and distribution but also on the particle shape and viscosity.

DOI: 10.1021/acsomega.6b00175
ACS Omega 2016, 1, 636−647

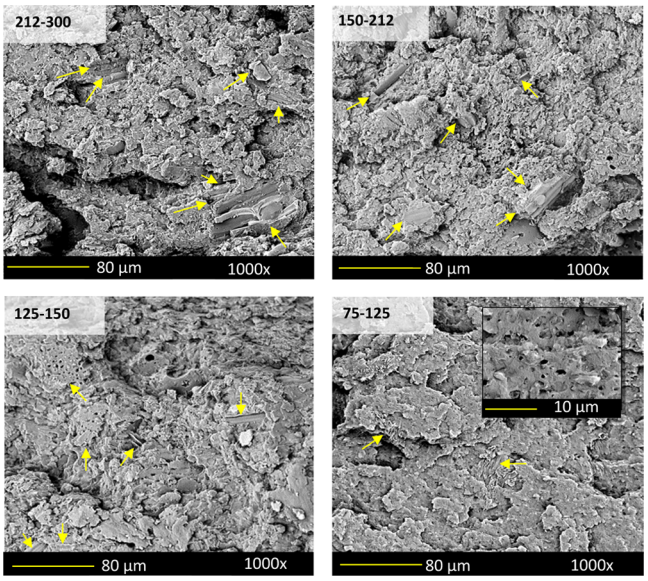

Figure 6. Morphology of composites with different size-fractionated biocarbon (the arrows point to biocarbon particles).

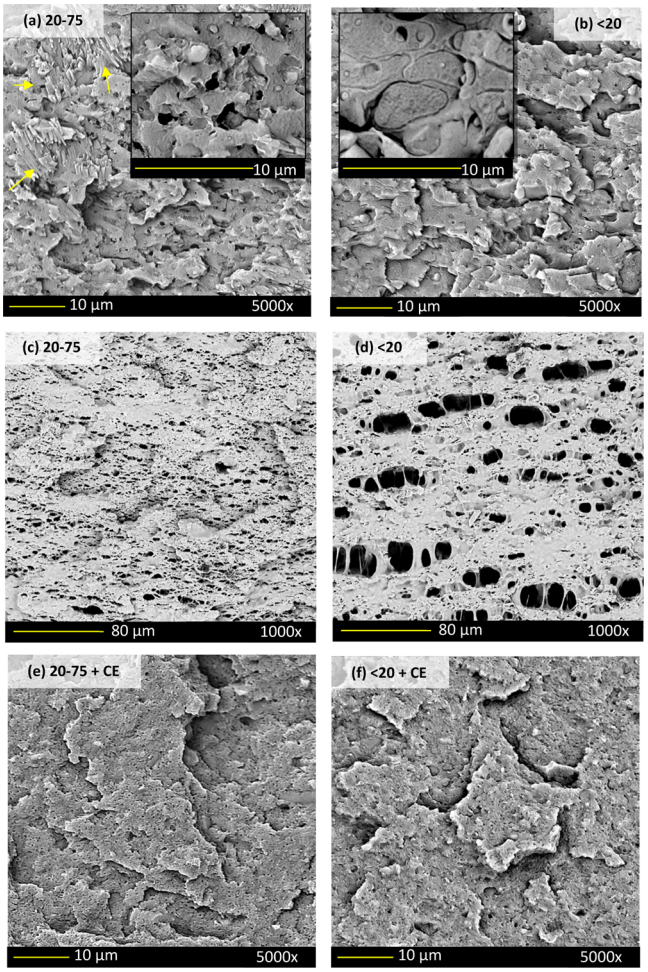

Figure 7. Morphology of composites with (a) 20−75 μm BC; (b) <20 μm BC; (c) 20−75 μm BC after etching; (d) <20 μm BC after etching; (e) 20−75 μm BC and 0.5 phr CE; and (f) <20 μm BC and 0.5 phr CE.

The effect of chain extender was assessed only in composites with 20−75 μm BC and less than 20 μm BC for simple comparison. On addition of CE to these composites, the morphology changed again; the dispersed domain sizes were further reduced to very small size, most likely because of the change in viscosity and interfacial tension between the dispersed blend components. The epoxy-based chain extender has been effective in breaking down the PLA phase to very small particles in both the composite formulations. The addition of CE was able to promote droplet breakup and overcome the effect of coalescence observed in less than 20 μm biocarbon composites. The fine dispersion of the particles in the matrix helps in increasing the toughness because the interparticle distance or the ligament thickness is reduced, facilitating yielding of the matrix.[26] Because the matrix used is a ternary blend system, it is important to control the blend inclusion size to achieve the desired morphologies, which will decide the majority of macroscopic properties. The effect of colloidal particles on stabilizing the morphology of emulsions has been an intense field of investigation for more than a century. Immiscible polymer blends are like highly viscous emulsions. Addition of nanofillers has been found to suppress the coarsening process and to stabilize the cocontinuous structure of the blends through accumulation at the interface. On the basis of this strategy, many nanofillers including carbon black have been used to stabilize the cocontinuous morphology.[27,28] Lipatov et al.[29] proposed that fillers can stabilize the blend morphology by adsorbing either of the blending polymers on their surface. In order for this interfacial stabilization to occur, the inorganic fillers should have highest surface area and should be dispersed very well in the blend. On the basis of our morphological observations, biocarbon with less than 20 μm is expected to have a high surface area when compared with other particle size ranges, which could help in suppressing the breakup of polymer particles. However, the addition of chain extender overpowers this suppression effect and facilitates very fine dispersion of PLA−EMAGMA particles in the matrix.

Mechanical Properties and HDT. Mechanical properties and HDT data for the PTT−PLA/EMAGMA blend (control) and the various biocarbon composites are presented in Figures 8 and 9. Baseline data for PTT/PLA (70/30) blend can be found in our previous study.[21] Incorporation of particulate fillers can modify the mechanical properties of polymers in many ways depending on the particle size, loading, particle−matrix interfacial adhesion, and the microstructure of the composites.[30] The maximum strength sustained by microparticulate composites under uniaxial tensile loading depends on the effective stress transfer between the matrix and filler particles. The biocarbon composites studied in this study did not show drastic improvements in tensile strength as the particle size range reduced; the results are shown in Figure 8. However, a slightly increasing trend is observed but with the values still being lower than the matrix strength. With the addition of CE and because of the high molding temperature (90 °C), the tensile strength of the composite is close to that of the blend processed at 30 °C. In addition to the chain extension effect, Joncryl has been reported to increase the viscosity and reduce the interfacial tension between the blending components, thus reducing the size of the dispersed phase, in this case PLA and EMAGMA. From morphological examinations discussed in the previous section, reduction in the dispersed phase size was found to be true for these blends. PLA with

DOI: 10.1021/acsomega.6b00175
ACS Omega 2016, 1, 636−647

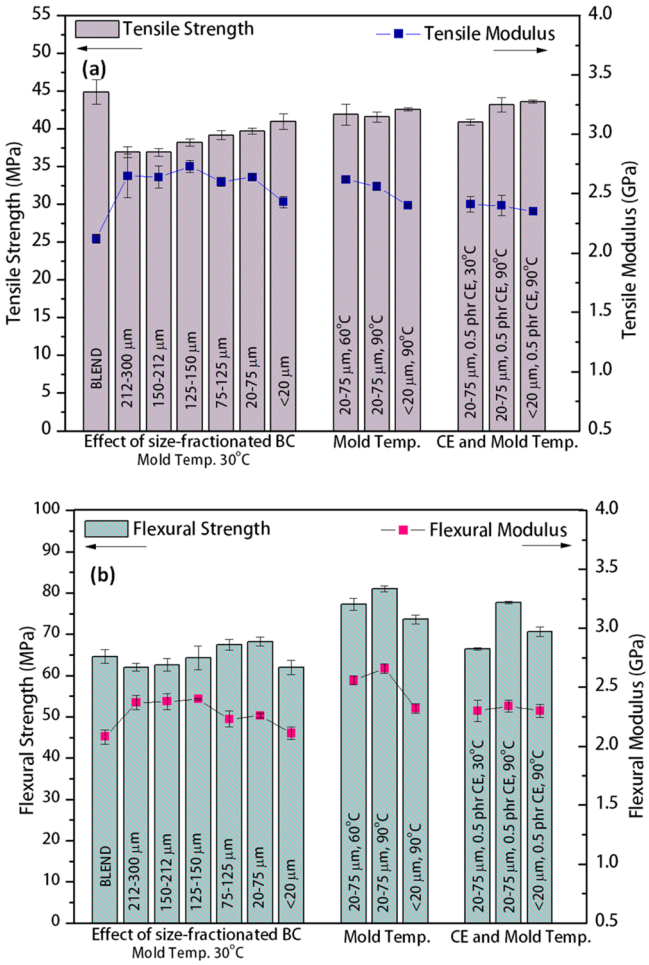

Figure 8. (a) Tensile and (b) flexural properties of size-fractionated biocarbon composites, showing the effect of varying size range, mold temperature, and CE.

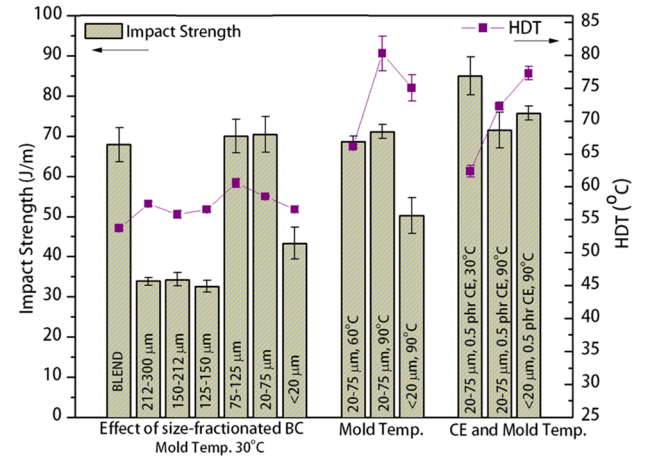

Figure 9. Impact strength and HDT for biocarbon composites.

reduced phase size in the PTT blend could act as efficient hard filler particles having relatively stronger adhesion with the matrix compared with the biocarbon particles, thereby increasing the stress transfer.

Flexural strength is the ability of a material to resist deformation under a combination of compressive and tensile stresses. Hence, values reported for flexural strength are usually higher than the tensile strength. From Figure 8b, considering the standard deviation, flexural strength remains almost the same for the biocomposites. The flexural strength of composites containing less than 20 μm BC was observed to decrease in comparison with composites with 20−75 μm BC. This anomalous observation can be explained with reference to the morphology of the composites containing less than 20 μm biocarbon. The coalesced bands of PLA−EMAGMA probably resulted in more flexibility, thus reducing the overall ability of composites to resist deformation. Prominent increase in the flexural strength is observed when the mold temperature is increased from 30 to 60 °C and then to 90 °C in 20−75 μm BC composites. This could be related to the increase in the crystallinity of PTT, which enhances secondary bonding through closely packed molecular chains.[31]

Addition of 10 wt % biocarbon has increased the tensile and flexural modulus of the composites. However, the modulus was observed to be not affected by the difference in the particle size range of biocarbon. It is not surprising because several studies in the literature have reported similar observations.[32,33] However, there are some theoretical predictions and experimental proofs that report an increase in modulus when the particle size is roughly below 30 nm.[34,35] On the basis of these observations, there seems to be a critical particle size beyond which there is no effect on composite modulus. As observed previously, the particle size of biocarbon is well above the 30 nm range proposed; hence, the modulus of biocomposites fabricated in this study is insensitive to the difference in the range of particle size examined. When the mold temperature was increased to enhance the crystallization rate of PTT, flexural modulus values increased, indicating the increase in stiffness of the composites. When CE was added to composites containing 20−75 and less than 20 μm BC, initial reduction in modulus, especially in flexural modulus was observed. When the mold temperature was increased to 90 °C, similar to the previous observation in composites without CE, the flexural modulus slightly increased.

For composites, impact strength is a complex correlation because of the presence of the orientation and distribution of fillers, the filler−matrix adhesion, and the resulting morphology. To have high impact strength or toughness, a large volume of the material should be able to absorb the energy dissipated. Values of impact strength observed are usually correlated with the energy dissipation mechanism preferred by the fracturing surface. Crack initiation and propagation are important in determining the impact strength of the composites. The same mechanism of pull-out and debonding, which increases the impact strength of composites, tends to have a negative effect on breaking strength. This is sometimes the reason for the inverse relationship between breaking strength and impact strength. Figure 9 shows the initial reduction in notched Izod impact strength, indicating the decreased ease of crack initiation and propagation in the presence of larger biocarbon particles. Impact-fractured surface morphology revealed a change in morphology as the size of the biocarbon particles reduced. As the blend components were dispersed in the matrix, impact strength increased, showing values closer to the level of the matrix. An impact strength of 70 J/m was achieved in the case of composites with 75−125 and 20−75 μm BC. Corroborating with morphological observations, the impact strength of composites with less than 20 μm biocarbon dropped to 40 J/m. This again can be attributed to the inability of the coalesced

DOI: 10.1021/acsomega.6b00175
ACS Omega 2016, 1, 636−647

structure to dissipate much energy or the absence of resistance to crack propagation and crack pinning effect.

With the addition of CE to composites containing 20−75 μm and less than 20 μm biocarbon, the impact strength increased to 85 J/m. This again could be related to the very fine dispersed polymer particle morphology observed in the presence of CE, which favored a high energy dissipating mechanism. When a suitable interparticle distance between the dispersed polymers is reached, the matrix can yield easily, thus improving impact strength. Another possible toughening mechanism is crack pinning. The finely dispersed and well-bonded PLA particles can facilitate the crack-pinning mechanism by impeding crack propagation. The crack tends to bow out between particles and forms secondary cracks that consume extra energy. This toughening mechanism has been noted in epoxy filled with rigid glass spheres.[36]

As the crystallization of PTT is promoted by increasing the mold temperature, impact strength of the composites containing 20−75 μm BC remained the same. However, in the presence of CE, samples molded at 90 °C showed reduction in the impact strength. An increase in crystallinity sometimes negatively affects the impact strength when the crystallites act as stress concentrators. It causes the stress acting on a small volume of the material to grow much higher than the average stress applied to the entire sample.[37] It is possible that this behavior is prominent only in the presence of CE because of the dispersion of PLA−EMAGMA in very small and fine particles. In addition to the crystalline structure, the crystalline superstructure that includes the spherulite size, crystalline form, and percentage crystallinity also influences the mechanical properties of semicrystalline polymers.[38]

Figure 9 also shows the HDT for the matrix and composites with different size-fractionated biocarbon. Incorporation of fillers is known to increase the HDT of semicrystalline polymers depending on the type of polymer and its crystallization rate, type, and the amount of filler loading. It also depends on processing conditions such as mold temperature that affect the mechanical behavior and the presence of nucleating agents enhancing crystallization. HDT is closely related to the flexural modulus of the filled composite.[31] The addition of different size-fractionated biocarbon has increased the HDT of the composites by at most 4−7 °C. This temperature is still very low for any engineering-polymer-based material to be stated as an upper value of dimensional stability. Therefore, the effect of mold temperature in increasing the crystallization and HDT was investigated. The gradual increase in flexural modulus noticed while increasing the mold temperature from 30 to 90 °C corresponds with the increment observed in HDT. A highest average HDT of 80 °C was obtained for composites with 20−75 μm and less than 20 μm molded at 90 °C. The improvement in HDT values at higher mold temperatures is attributed to the enhanced stiffness and percentage of PTT crystallization. The effect of 60 °C mold temperature on less than 20 μm BC was not studied because results from the 20−75 μm BC composites showed that the temperature 90 °C provided the highest improvement in the HDT value.

Rheology. Incorporation of solid particulates can critically alter the flow characteristics, influencing melt processing and the properties of the final composites.[39] Key factors changing the rheological behavior of composites are filler size, shape, concentration, and the interactions between filler particles.[40] In general, for a composite system, viscosity increases with filler concentrations and reduction in filler particle size. Fillers with a smaller particle size facilitate the formation of filler network or structural skeleton within the polymer matrix, resulting in a very sharp rise in viscosity at a low shear rate. Defining yield stress behavior has been reported for nanoparticles forming such network structures.[41] Yield stress is not observed in polymers filled with larger particles because the hydrodynamic interaction dominates the response to shear deformation rather than particle−particle interaction.[41] As the material is subjected to higher shear rate, the filler network structure is destroyed and the effect of filler on viscosity becomes minimal.[42]

Figure 10 shows the dependence of viscosity, η, on log shear rate, $\dot{\gamma}$. The PTT blend matrix exhibits zero shear viscosity

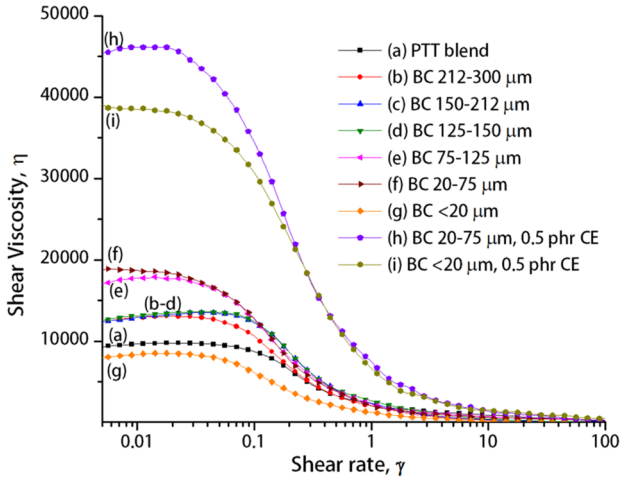

Figure 10. Shear rate vs viscosity for size-fractionated biocarbon composites.

plateau, indicating Newtonian behavior at low shear rates and power-law behavior at higher shear rates. Upon the addition of size-fractionated biocarbon (up to 75 μm), viscosity of the composites in the limit of Newtonian region was observed to increase. The highest viscosity was achieved at 20−75 μm range, implying that there is tighter packing between particles potentially resisting relative motion. Surprisingly, with further reduction in the particle size, the viscosity of the composites dropped below the matrix viscosity. It is important to mention that this reduction in viscosity was reproducible.

Such conspicuous reduction in viscosity has been reported previously for polymer composites with nanoparticles.[41] Dilution of the polymer chain entanglement density, selective adsorption of high-molecular-weight polymer chains on the surface of the particles, increased excluded free volume induced around the particles, slip between the sample and the geometry during rheological testing, and the degradation of the matrix are some of the reasons attributed to this behavior.[41] Smoother particles tend to exhibit a lower shear viscosity when compared with uneven and sharp particles. The change in shape of the <20 μm particles because of milling could also be one possible reason for such reduction in viscosity. Extended set of experimental results is required to precisely conclude which of these factors are responsible for the observed reduction in viscosity of the <20 μm BC composites.

At higher shear rates, the chains can disentangle, orient, or stretch themselves parallel to the direction of driving force. Therefore, in a nonlinear region, the sample is deformed to a point wherein the molecular structure is destroyed and shear

DOI: 10.1021/acsomega.6b00175
ACS Omega 2016, 1, 636−647

Table 1. Differential Scanning Calorimetry Data

composite formulations	T_g (°C)		T_m (°C)		H_m (J/g)		T_{cc} (°C)		H_{cc} (J/g)		T_c (°C)	% crys
	PTT	PLA	PTT	PLA	PTT	PLA	PTT	PLA	PTT	PLA	PTT	PTT
PTT blend, 30 °C mold	43.42	55.8	226.5	164.8	33.0	7.4	68.1	103.3	11.3	2.5	193.0	24.9
Effect of Size-Fractionation at Mold Temperature of 30 °C												
BC 212−300 μm	48.1	56.5	227.0	163.1	36.0	8.0	69.5	100.8	4.7	4.5	201.2	40.1
BC 150−212 μm	46.7	57.3	228.7	164.5	32.2	5.0	70.1	101.7	2.8	4.5	202.8	37.7
BC 125−150 μm	47.0	57.0	228.2	164.7	32.1	8.0	69.8	103.6	5.4	3.0	200.4	34.2
BC 75−125 μm	50.5	58.6	226.7	166.0	30.1	7.5	67.7	100.9	9.7	2.1	199.4	26.1
BC 20−75 μm	45.3	57.8	228.9	166.3	30.1	7.6	69.3	100.3	11.9	1.9	200.8	23.1
BC <20 μm	49.2	59.6	228.1	165.6	28.0	7.0	69.1	102.3	12.0	2.8	199.4	20.6
Effect of Mold Temperature												
BC 20−75 μm, 60 °C	46.0	60.6	228.1	165.7	31.7	7.2	67.5	103.6	0.2	0.9	197.6	40.4
BC 20−75 μm, 90 °C	46.5	60.2	227.2	165.5	31.0	6.9		104.1		2.5	198.0	39.7
BC <20 μm, 90 °C	46.6	59.8	226.9	165.0	28.8	7.6		103.3		2.8	196.1	36.9
Effect of CE and Mold Temperature												
BC 20−75 μm, 0.5 phr CE 30 °C mold	45.6	60.5	227.5	164.7	29.7	5.8	69.1	107.7	10.1	1.9	200.7	22.7
BC 20−75 μm, 0.5 phr CE 90 °C mold	46.6	60.7	227.0	164.9	27.2	4.7		109.2		1.2	198.2	34.9
BC <20 μm, 0.5 phr CE 90 °C mold	46.1	60.1	227.6	163.7	28.0	6.0		106.2		2.7	196.7	35.9

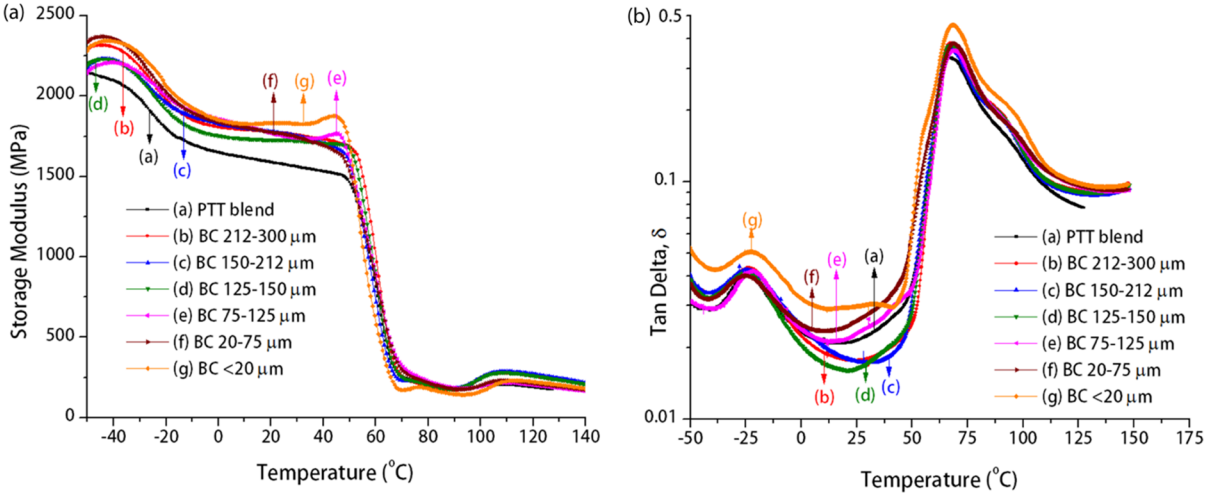

Figure 11. (a) Storage modulus and (b) tan δ graphs for PTT biocomposites with size-fractionated biocarbon.

thinning takes place with a drastic drop in viscosity. In summary, the incorporation of biocarbon affects the viscosity based on the particle size and shape at low shear rates, but the basic shear thinning behavior of the polymer matrix is not affected. The observed increase or decrease in viscosity of the composites at low shear rates depends on the polymer inclusion phase present in the matrix and on how they are affected based on the particle size range of biocarbon.

Thermal Properties. *Differential Scanning Calorimetry (DSC).* The nonisothermal crystallization behavior of PTT blend and biocomposites was studied using differential scanning calorimetry (DSC) to investigate the effect of size-fractionation, mold temperature, and chain extender. Table 1 shows the values obtained for glass transition temperature (T_g), melting temperature (T_m) and the corresponding enthalpy (H_m), cold crystallization temperature (T_{cc}) and the corresponding enthalpy (H_{cc}) from the first heating cycle, and crystallization temperature (T_c) from the cooling cycle. T_g values of PTT and PLA in biocomposites have increased slightly with the addition of biocarbon and CE and the increase in mold temperature when compared with the T_g values of these components in the blend. The addition of size-fractionated biocarbon and CE and the change in mold temperature have slowed down the local dynamics of polymer chain, hence the increase in T_g of PTT and PLA in composites. Average melting temperatures for PTT and PLA remained the same throughout the entire range of formulations tested.

Although T_{cc} values of PTT and PLA remained the same, an interesting trend was observed in the enthalpy values (H_{cc}). As the particle size range of biocarbon decreased, H_{cc} of PTT increased and that of PLA decreased. A larger fraction of PTT chains were not able to crystallize during the molding process as the biocarbon particle size and the inclusion phase size decreased. However, T_{cc} of PTT disappeared with increase in mold temperature, indicating faster and complete crystallization of PTT achieved during high temperature molding. PLA exhibited its characteristic cold crystallization temperature at around 100 °C. Increase in this temperature to ∼110 °C indicated a slower crystallization rate in the presence of chain extender. Increase in mold temperature did not seem to have any effect on T_{cc} of PLA. Previously, we discovered the T_{cc} of PLA to disappear only at a mold temperature of 120 °C.[43]

As expected, the PLA phase did not exhibit melt crystallization upon cooling because of its very slow

DOI: 10.1021/acsomega.6b00175
ACS Omega 2016, 1, 636−647

crystallization rate. The T_c value of PTT in certain composite formulations was increased, compared with the value observed for the blend. Percentage crystallinity calculated for composites with different size-fractionated biocarbon is observed to decrease with a decrease in the particle size range. This is expected as the cold crystallization enthalpy increased. Increase in the mold temperature for composites with 20−75 μm and <20 μm BC increased the crystallinity by 20%, and this was directly reflected in the HDT values. Although composites with BC >150 μm had similar high values of crystallinity, the HDT values were observed to be low. As the mold temperature increased, it is possible that the higher fraction of amorphous chains were arranged closer to the crystalline fraction. Consequently, this arrangement hinders free movement of the entire long chain, resists heat-induced distortions, resulting in enhanced HDT.

Dynamic Mechanical Analysis. Storage modulus (G') and damping factor (tan δ) for different size-fractionated biocarbon against temperature are shown in Figure 11. Overlaid storage modulus and tan δ graphs for 20−75 μm biocarbon in the presence of CE and at different mold temperatures are shown in Figure 12. The first obvious observation is the increase in storage modulus of the composites compared with that of the blend matrix because of the addition of biocarbon. All of the composites showed similar values of storage modulus. A drop in storage modulus in subzero temperatures is characterized by the transition of EMAGMA phase in the blends and composites. At the plateau region above 0 °C and below T_g, rapid short range diffusion motions dependent on the chain entanglement take place. A drastic drop in storage modulus occurs when the material passes through the T_g values of PTT and PLA, showing an α transition relaxation peak.

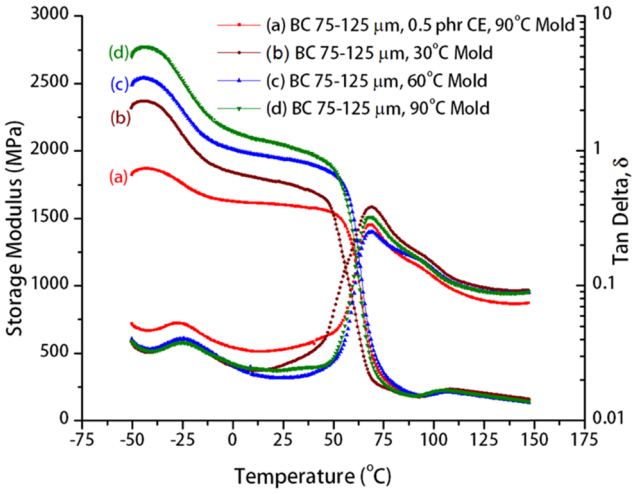

Figure 12. Storage modulus and tan δ graphs for PTT biocomposites with 20−75 μm biocarbon.

Beyond 90 °C, transitions assigned to the polymer chain rearrangement in the crystalline domain and across the amorphous-crystal interphase occur. This temperature coincides well with the cold crystallization temperature observed for PLA using DSC. Composites with 20−75 μm biocarbon containing CE showed reduced storage modulus, with values less than that of the matrix. As the mold temperature was increased from 30 to 90 °C, a gradual step increase in storage modulus was observed corroborating with other test results. The vertical magnitude of the tan δ peak gives information regarding the damping behavior of the biocarbon on the motion of polymer chains. Reduction in the tan δ peak indicates restricted molecular movement due to polymer−particle interactions. In our case, the peak height was only slightly varied between different size-fractionated biocarbon, and at less than 20 μm BC, the magnitude of the tan δ peak was higher than that of the matrix. This particular composite seems to have experienced higher viscoelastic energy dissipation. Composites with 20−75 μm BC at higher mold temperature showed greater degree of damping when compared with the ones molded at 30 °C.

CONCLUSIONS

In this study, biocomposites were made from PTT 70/PLA 30−EMAGMA blend (85−15) and 10 wt % biocarbon. Biocarbon between size ranges of 212−300, 150−212, 125−150, 75−125, 20−75, and <20 μm was fractionated using Tyler sieves having corresponding sieve-opening size. Important findings from this study are summarized below. The blend matrix retained its primary sea-island morphology with roughly spherical domains of the PLA−EMAGMA dispersed phase in composites with 75−125 and 20−75 μm biocarbon. At larger particle size range, biocarbon offered hindrance to the dispersion of the blend components during processing. Further change in the morphology of composites with <20 μm biocarbon was attributed to the good dispersion of the particles that could stabilize the blend morphology, showing coalesced PLA−EMAGMA particles. Addition of chain extender was effective in suppressing the coalescence and dispersed the PLA−EMAGMA particles in much smaller and finer morphologies. This morphology was favorable in achieving a higher impact strength by a combination of yielding and crack-pinning mechanism. In an attempt to improve the crystallinity of PTT, the mold temperature was increased. This promoted faster PTT crystallization, consequently increasing the HDT to around 80 °C in some of the formulations when the mold temperature was 90 °C. The stiffening effect achieved with increasing mold temperature was further supported by the increase in flexural modulus. The viscosity of different polymers measured from rheological tests supported the morphology and mechanical properties observed for the biocomposites. In summary, this study showed that using biocarbon having appropriate size and shape, morphology of the composites can be controlled and that by increasing the mold temperature, favorable improvement in crystallinity can be obtained. In addition to achieving the desired properties, cost reduction involved in using biocarbon can also contribute to the success of these composites in finding high performance applications.

ASSOCIATED CONTENT

Supporting Information

The Supporting Information is available free of charge on the ACS Publications website at DOI: 10.1021/acsomega.6b00175.

Fourier transform infrared spectroscopy (FTIR) for biocarbon (PDF)

AUTHOR INFORMATION

Corresponding Author

*E-mail: mohanty@uoguelph.ca. Phone:+1-519-824-4120 ext. 56664. Fax: +1-519-763-8933 (A.K.M.).

Notes

The authors declare no competing financial interest.

DOI: 10.1021/acsomega.6b00175
ACS Omega 2016, 1, 636−647

■ ACKNOWLEDGMENTS

The authors gratefully acknowledge the financial support from (1) the Ontario Ministry of Agriculture, Food, and Rural Affairs (OMAFRA)—University of Guelph Bioeconomy-Industrial Uses Theme (Project # 200245, 200358, 200425); (2) the Ontario Research Fund, Research Excellence Program; Round-7 (ORF-RE07) from the Ontario Ministry of Research and Innovation (MRI), currently known as the Ontario Ministry of Research, Innovation and Science (MRIS) (Project # 052644 and # 052665); (3) the Natural Sciences and Engineering Research Council (NSERC) Canada Discovery Grants (Project # 401111); and (4) the NSERC Network of Centres of Excellence (NCE) AUTO21 Program (Project # 460372 and 460373).

■ REFERENCES

(1) *Scientific Consensus: Earth's Climate is Warming*. http://climate.nasa.gov/scientific-consensus/ (accessed July 14, 2016).
(2) *International Biochar Initiative: Standardized Product Definition and Product Testing Guidelines for Biochar that is Used in Soil*. http://www.biochar-international.org/sites/default/files/IBI_Biochar_Standards_V2%200_final_2014.pdf (accessed July 14, 2016).
(3) Schmidt, H.-P. 55 uses of biochar. *Ithaka Journal for Ecology, Winegrowing and Climate Farming* **2012**, *1*, 286−289.
(4) Das, O.; Sarmah, A. K.; Bhattacharyya, D. A sustainable and resilient approach through biochar addition in wood polymer composites. *Sci. Total Environ.* **2015**, *512*, 326−336.
(5) Peterson, S. C.; Chandrasekaran, S. R.; Sharma, B. K. Birchwood biochar as partial carbon black replacement in styrene−butadiene rubber composites. *J. Elastomers Plast.* **2016**, *48*, 305−316.
(6) Peterson, S. C. Utilization of low-ash biochar to partially replace carbon black in styrene−butadiene rubber composites. *J. Elastomers Plast.* **2013**, *45*, 487−497.
(7) Peterson, S. C. Evaluating corn starch and corn stover biochar as renewable filler in carboxylated styrene−butadiene rubber composites. *J. Elastomers Plast.* **2012**, *44*, 43−54.
(8) Jong, L.; Peterson, S. C.; Jackson, M. A. Utilization of porous carbons derived from coconut shell and wood in natural rubber. *J. Polym. Environ.* **2014**, *22*, 289−297.
(9) Behazin, E.; Ogunsona, E.; Rodriguez-Uribe, A.; Mohanty, A. K.; Misra, M.; Anyia, A. O. Mechanical, Chemical, and Physical Properties of Wood and Perennial Grass Biochars for Possible Composite Application. *BioResources* **2015**, *11*, 1334−1348.
(10) Anstey, A.; Vivekanandhan, S.; Rodriguez-Uribe, A.; Misra, M.; Mohanty, A. K. Oxidative acid treatment and characterization of new biocarbon from sustainable Miscanthus biomass. *Sci. Total Environ.* **2016**, *550*, 241−247.
(11) Myllytie, P.; Misra, M.; Mohanty, A. K. Carbonized Lignin as Sustainable Filler in Biobased Poly(trimethylene terephthalate) Polymer for Injection Molding Applications. *ACS Sustainable Chem. Eng.* **2016**, *4*, 102−110.
(12) Zaverl, M. J.; Misra, M.; Mohanty, A. K. Using factorial statistical method for optimising co-injected biochar composites. *The Proceedings of the 19th International Conference on Composite Materials*, 2013, *11*; pp 7802−7809.
(13) Huber, T.; Misra, M.; Mohanty, A. K. Biochar and Its Size Effects on Polyamide 6/Biochar Composites. *Proceedings of the American Society for Composites 30th Conference*, 2015; pp 1531−1538.
(14) Mohanty, A. K.; Vivekanandhan, S.; Anstey, A.; Misra, M. Sustainable composites from renewable biochar and engineering plastics. *Proceedings of 20th International Conference on Composite Materials*, 2015, pp 4308−4312.
(15) Ahmetli, G.; Kocaman, S.; Ozaytekin, I.; Bozkurt, P. Epoxy composites based on inexpensive char filler obtained from plastic waste and natural resources. *Polym. Compos.* **2013**, *34*, 500−509.
(16) Nan, N.; DeVallance, D. B.; Xie, X.; Wang, J. The effect of bio-carbon addition on the electrical, mechanical, and thermal properties of polyvinyl alcohol/biochar composites. *J. Compos. Mater.* **2016**, *50*, 1161−1168.
(17) DeVallance, D. B.; Oporto, G. S.; Quigley, P. Investigation of hardwood biochar as a replacement for wood flour in wood−polypropylene composites. *J. Elastomers Plast.* **2016**, *48*, 510−522.
(18) Das, O.; Sarmah, A. K.; Bhattacharyya, D. A novel approach in organic waste utilization through biochar addition in wood/polypropylene composites. *Waste Manage.* **2015**, *38*, 132−140.
(19) Das, O.; Sarmah, A. K.; Bhattacharyya, D. Biocomposites from waste derived biochars: Mechanical, thermal, chemical, and morphological properties. *Waste Manage.* **2016**, *49*, 560−570.
(20) Das, O.; Sarmah, A. K.; Zujovic, Z.; Bhattacharyya, D. Characterisation of waste derived biochar added biocomposites: Chemical and thermal modifications. *Sci. Total Environ.* **2016**, *550*, 133−142.
(21) Nagarajan, V.; Mohanty, A. K.; Misra, M. Reactive compatibilization of poly trimethylene terephthalate (PTT) and polylactic acid (PLA) using terpolymer: Factorial design optimization of mechanical properties. *Mater Des.* **2016**, *110*, 581−591.
(22) Pyda, M.; Boller, A.; Grebowicz, J.; Chuah, H.; Lebedev, B. V.; Wunderlich, B. Heat capacity of poly(trimethylene terephthalate). *J. Polym. Sci., Part B: Polym. Phys.* **1998**, *36*, 2499−2511.
(23) Miao, Z.; Grift, T. E.; Hansen, A. C.; Ting, K. C. Energy requirement for comminution of biomass in relation to particle physical properties. *Ind. Crops Prod.* **2011**, *33*, 504−513.
(24) *ASTM F1877-05. Standard Practice for Characterization of Particles*. http://compass.astm.org/EDIT/html_annot.cgi?F1877+05\(2010\).
(25) Igathinathane, C.; Pordesimo, L. O.; Columbus, E. P.; Batchelor, W. D.; Sokhansanj, S. Sieveless particle size distribution analysis of particulate materials through computer vision. *Comput. Electron. Agric.* **2009**, *66*, 147−158.
(26) Wu, S. Phase structure and adhesion in polymer blends: A criterion for rubber toughening. *Polymer* **1985**, *26*, 1855−1863.
(27) Gubbels, F.; Blacher, S.; Vanlathem, E.; Jerome, R.; Deltour, R.; Brouers, F.; Teyssie, P. Design of electrical composites: Determining the role of the morphology on the electrical properties of carbon black filled polymer blends. *Macromolecules* **1995**, *28*, 1559−1566.
(28) Tan, Y.; Song, Y.; Cao, Q.; Zheng, Q. Characterization of carbon black-filled immiscible polypropylene/polystyrene blends. *Polym. Int.* **2011**, *60*, 823−832.
(29) Lipatov, Y. S.; Nesterov, A.; Ignatova, T.; Nesterov, D. A. Effect of polymer−filler surface interactions on the phase separation in polymer blends. *Polymer* **2002**, *43*, 875−880.
(30) Fu, S.-F.; Feng, X.-Q.; Lauke, B.; Mai, Y.-W. Effects of particle size, particle/matrix interface adhesion and particle loading on mechanical properties of particulate−polymer composites. *Composites, Part B* **2008**, *39*, 933−961.
(31) Landel, R. F.; Nielsen, L. E. *Mechanical Properties of Polymers and Composites*, 2nd ed.; Marcel Decker Inc: New York, 1993.
(32) Xie, X.; Mai, Y.; Zhou, X. Dispersion and alignment of carbon nanotubes in polymer matrix: A review. *Mater. Sci. Eng., R* **2005**, *49*, 89−112.
(33) Suprapakorn, N.; Dhamrongvaraporn, S.; Ishida, H. Effect of $CaCO_3$ on the mechanical and rheological properties of a ring-opening phenolic resin: Polybenzoxazine. *Polym. Compos.* **1998**, *19*, 126−132.
(34) Ji, X. L.; Jing, J. K.; Jiang, W.; Jiang, B. Z. Tensile modulus of polymer nanocomposites. *Polym. Eng. Sci.* **2002**, *42*, 983−99SS.
(35) Mishra, S.; Sonawane, S. H.; Singh, R. P. Studies on characterization of nano $CaCO_3$ prepared by the in situ deposition technique and its application in PP-nano $CaCO_3$ composites. *J. Polym. Sci., Part B: Polym. Phys.* **2005**, *43*, 107−113.
(36) Maxwell, D.; Young, R. J.; Kinloch, A. J. Hybrid particulate-filled epoxy-polymers. *J. Mater. Sci. Lett.* **1984**, *3*, 9−12.
(37) Kfoury, G.; Raquez, J.-M.; Hassouna, F.; Odent, J.; Toniazzo, V.; Ruch, D.; Dubois, P. Recent advances in high performance poly (lactide): from "green" plasticization to super-tough materials via (reactive) compounding. *Front Chem.* **2013**, *1*, 1−46.

DOI: 10.1021/acsomega.6b00175
ACS Omega 2016, 1, 636−647

(38) Karger-Kocsis, J. Microstructural aspects of fracture in polypropylene and in its filled, chopped fiber and fiber mat reinforced composites. In *Polypropylene Structure, Blends and Composites*; 1st ed.; Chapman & Hall: London, 1995; pp 142−201.
(39) Katz, H. S. Particulate fillers. In *Handbook of Composites*, 2nd ed.; Peters, S. T., Ed.; Springer Science & Business Media: Dordrecht, 2013; pp 242−253.
(40) Poslinski, A. J.; Ryan, M. E.; Gupta, R. K.; Seshadri, S. G.; Frechette, F. J. Rheological Behavior of Filled Polymeric Systems I. Yield Stress and Shear-Thinning Effects. *J. Rheol.* **1988**, *32*, 703−735.
(41) Tan, H.; Lin, Y.; Zheng, J.; Gong, J.; Qiu, J.; Xing, H.; Tang, T. Particle-size dependent melt viscosity behavior and the properties of three-arm star polystyrene−Fe_3O_4 composites. *Soft Matter* **2015**, *11*, 3986−3993.
(42) Shenoy, A. V. *Rheology of Filled Polymer Systems*; Springer Science & Business Media: Dordrecht, 2013.
(43) Nagarajan, V.; Zhang, K.; Misra, M.; Mohanty, A. K. Overcoming the Fundamental Challenges in Improving the Impact Strength and Crystallinity of PLA Biocomposites: Influence of Nucleating Agent and Mold Temperature. *ACS Appl. Mater. Interfaces* **2015**, *7*, 11203−11214.

DOI: 10.1021/acsomega.6b00175
ACS Omega 2016, 1, 636−647